Received: 17 January 2022 | Revised: 24 March 2022 | Accepted: 26 March 2022

DOI: 10.1111/cas.15351

ORIGINAL ARTICLE

Cancer Science WILEY

circ_0006089 promotes gastric cancer growth, metastasis, glycolysis, and angiogenesis by regulating miR-361-3p/TGFB1

Ying Zhou[1] | Qilin Zhang[2] | Bingling Liao[1] | Xiaofeng Qiu[2] | Sheng Hu[2] | Qihua Xu[1]

[1]Department of Gastroenterology, Seventh People's Hospital of Shanghai University of Traditional Chinese Medicine, Shanghai, China

[2]Department of General Surgery, Seventh People's Hospital of Shanghai University of Traditional Chinese Medicine, Shanghai, China

Correspondence
Qihua Xu, Department of Gastroenterology, Seventh People's Hospital of Shanghai University of Traditional Chinese Medicine, No. 358 Datong Road, Pudong New District, Shanghai 200120, China.
Email: xuqihua0913@126.com

Funding Information
This study was supported by Excellent Young Medical Talent in the Health System of Pudong new district [PWRq2020-23]; the Science and Technology Development Fund of Pudong, China [PKJ2020-Y15]; and the Talents Training Programme of the Seventh People's Hospital of Shanghai University of TCM [XX2019-07]

Abstract

Circular RNA (circRNA) participates in a variety of pathophysiological processes, including the development of gastric cancer (GC). However, the role of circ_0006089 in GC progression and its underlying molecular mechanism need to be further revealed. Quantitative real-time PCR was utilized for detecting circ_0006089, microRNA (miR)-361-3p and transforming growth factor-β1 (TGFB1) expression. The interaction between miR-361-3p and circ_0006089 or TGFB1 was confirmed using a dual-luciferase reporter assay and an RNA immunoprecipitation (RIP) assay. Cell proliferation, metastasis, apoptosis, and angiogenesis were determined using colony formation assay, EdU assay, transwell assay, flow cytometry, and tube formation assay. Cell glycolysis was evaluated by detecting glucose consumption, lactate production, and ATP levels. In addition, western blot (WB) analysis was used to measure protein expression. Xenograft tumor models were used to assess the effect of circ_0006089 knockdown on GC tumorigenesis. circ_0006089 had been found to be upregulated in GC tissues and cells, and it could act as an miR-361-3p sponge. circ_0006089 knockdown suppressed GC proliferation, metastasis, glycolysis, angiogenesis, and increased apoptosis, while this effect could be revoked by miR-361-3p inhibitor. TGFB1 was targeted by miR-361-3p, and its overexpression reversed the effects of miR-361-3p on GC cell function. Also, circ_0006089 promoted TGFB1 expression via sponging miR-361-3p. Animal experiments showed that silenced circ_0006089 inhibited GC tumorigenesis through the miR-361-3p/TGFB1 pathway. Our results revealed that the circ_0006089/miR-361-3p/TGFB1 axis contributed to GC progression, confirming that circ_0006089 might be a potential therapeutic target for GC.

KEYWORDS
circ_0006089, gastric cancer, miR-361-3p, TGFB1

Abbreviations: circRNA, circular RNA; GC, gastric cancer; GES-1, gastric mucosa cells; IHC, immunohistochemistry; miR, microRNA; qRT-PCR, quantitative real-time PCR; TGFB1, transforming growth factor-β; WB, Western blot.

Ying Zhou and Qilin Zhang contributed equally to this work.

1 | INTRODUCTION

Gastric cancer (GC) is a malignant tumor derived from the epithelium of gastric mucosa and has a high incidence worldwide.[1,2] Due to the low rate of early diagnosis, most patients with GC are already in the middle and advanced stages at the time of diagnosis, so the patient's prognosis is still not optimistic.[3,4] Targeted therapy can specifically target cancer cells and has little effect on normal cells, so it plays a vital role in cancer treatment, including GC.[5,6] Therefore, mining potential therapeutic targets of GC with clinical value is very important to improve the therapeutic effect of GC.

Circular RNAs (circRNAs) are a class of noncoding RNAs that have a closed loop structure formed by back splicing.[7,8] CircRNA participates in the regulation of gene expression through various mechanisms, among which one mechanism is that circRNA acts as a "molecular sponge" to complement with microRNAs (miRNA) and then inhibit their biological functions.[9,10] CircRNA is closely related to human disease development and has become an ideal molecular marker of cancer treatment.[11,12] Many circRNAs have been confirmed to participate in GC malignant progression. circ_0007505 was found to be an upregulated circRNA and it might be a potential treatment target for GC.[13] Also, circ_0006470 was considered to be an oncogene in GC that enhanced GC proliferation and migration through the miR-27b-3p/PI3KCA pathway.[14] Additionally, circPTK2 has been discovered to act as an miR-196-3p sponge to upregulate AATK, thereby inhibiting GC proliferation and metastasis.[15]

Through analyzing the Gene Expression Omnibus (GEO) database, we discovered that circ_0006089 was an obviously upregulated circRNA in GC tissues. Previous research revealed that the high expression of circ_0006089 restrained the malignant progression of cisplatin-resistant GC cells to affect the chemoresistance of GC.[16] However, the exact role of circ_0006089 in the progress of GC has not yet been confirmed. In view of previous studies, we speculated that circ_0006089 might participate in regulating GC progression as a cancer-promoting factor. Here, we explored the function of circ_0006089 knockdown on GC cell function and tumorigenesis and revealed its underlying molecular mechanism, in order to provide evidence for circ_0006089 to become a potential GC therapeutic target.

2 | MATERIALS AND METHODS

2.1 | Tissue samples

In total, 80 patients with GC were recruited from the Seventh People's Hospital of Shanghai University of Traditional Chinese Medicine. GC tumor tissues and matched adjacent normal tissues were stored at −80°C. Our study was approved by the Ethics Committee of Seventh People's Hospital of Shanghai University of Traditional Chinese Medicine, and all patients participating in the study signed written informed consents.

2.2 | Cell culture and transfection

Mycoplasma contamination is a common problem in cell culture. Our laboratory conducts regular mycoplasma tests to ensure that the cells are free from mycoplasma contamination. Human GC cells (AGS and HGC-27) and normal gastric mucosa cells (GES-1) were purchased from Procell (Wuhan, China) and cultured in RPMI-1640 medium (Gibco, Grand Island, NY, USA) containing 10% FBS and 1% penicillin/streptomycin at 37°C with 5% CO_2. Oligonucleotides and vectors were designed by RiboBio (Guangzhou, China) and were transfected into cells using Lipofectamine 3000 reagent (Invitrogen), including circ_0006089 small interfering RNA (si-circ_0006089#1: 5′- ACATCTGAGCTGCTGGCTAAC-3′; si-circ_0006089#2: 5′-AACATCTGAGCTGCTGGCTAA-3′, miR-361-3p mimic (5′-UCCCCCAGGUGUGAUUCUGAUUU-3′) or inhibitor (in-miR-361-3p: 5′-AAAUCAGAAUCACACCUGGGGGA-3′), and their negative controls (si-NC: 5′-UUCUCCGAACGUGUCACGUTT-3′; miR-NC: 5′-UUGUACUACACAAAAGUACUG-3′; in-miR-con: 5′-CAGUACUUUUGUGUAGUACAA-3′). After transfection for 48 h, cells were harvested for functional experiments. For overexpressing circ_0006089 and transforming growth factor-β1 (TGFB1), the sequences of circ_0006089 andTGFB1 were cloned into the pCD5 vector and the pcDNA vector by RiboBio Ltd. The overexpression vector was transfected into cells using Lipofectamine 3000.

2.3 | Quantitative real-time PCR (qRT-PCR)

TRIzol reagent (Invitrogen) was utilized for RNA extraction from tissues and cells, and PrimeScript RT reagent kit (Takara, Dalian, China) was utilized for synthesizing cDNA. Finally, cDNA and specific primers were mixed with SYBR Premix Ex *Taq*II (TaKaRa) to perform PCR reaction in a PCR system. Primer sequences are listed in Table 1. In this, β-actin or U6 was applied as internal control and data were analyzed using the $2^{-\Delta\Delta Ct}$ method. To evaluate the resistance of circ_0006089 to RNase R digestion, the RNA isolated from GC cells was incubated with RNase R and then used for qRT-PCR. To determine the distribution of circ_0006089 in the cell cytoplasm and nucleus, the RNAs from the cytoplasm and nucleus were isolated using the PARIS kit (Invitrogen), and then circ_0006089 expression was detected using qRT-PCR. Here, β-actin and U6 were used as the cytoplasm control and nuclear control, respectively.

2.4 | Dual-luciferase reporter assay

Basing on the binding sites between miR-361-3p and circ_0006089 or TGFB1 3′UTR, the wild-type and mutant-type fragments of circ_0006089 or TGFB1 3′UTR were ligated to the pGL3 reporter vectors by Genepharma (Shanghai, China), generating the circ_0006089-WT/MUT vectors or TGFB1 3′UTR-WT/MUT vectors. GC cells were co-transfected with the reporter vectors (circ_0006089-WT/MUT or TGFB1 3′UTR-WT/MUT) and miR-361-3p mimic or miR-NC for

TABLE 1 Primer sequences used for qRT-PCR

Name		Primers (5′–3′)
circ_0006089	Forward	AGTGTTCCGGAATCCACCGA
	Reverse	CTCCTCAGGGTTGGTCTTCAC
ASAP2	Forward	CCCATGAGGACTACAAGGCG
	Reverse	CATTTTCCACGTGAGCCAGC
TGFB1	Forward	ATGGAGAGAGGACTGCGGAT
	Reverse	TAGTGTTCCCCACTGGTCCC
miR−361-3p	Forward	GTATGATCCCCCAGGTGTGATTC
	Reverse	CTCAACTGGTGTCGTGGAG
miR−217	Forward	GTATGATACTGCATCAGGAACTG
	Reverse	CTCAACTGGTGTCGTGGAG
miR−616-3p	Forward	GTATGAAGTCATTGGAGGGTTT
	Reverse	CTCAACTGGTGTCGTGGAG
miR−223-3p	Forward	GTATGATGTCAGTTTGTCAAAT
	Reverse	CTCAACTGGTGTCGTGGAG
β-actin	Forward	GACTCCAAGGCCACGGATAG
	Reverse	TGTTCGAGGATCTGTGCCAA
U6	Forward	CTCGCTTCGGCAGCACA
	Reverse	AACGCTTCACGAATTTGCGT

48 h. Cell luciferase activity was detected using the Dual-Luciferase Reporter Gene Assay Kit (Beyotime, Shanghai, China).

2.5 | RNA immunoprecipitation (RIP) assay

The RNA Immunoprecipitation Kit (Geneseed, Guangzhou, China) was used. Briefly, GC cells cultured for 48 h were lysed using RIP lysis buffer. Cell extracts were treated with magnetic bead-coupled anti-Ago2 or anti-IgG overnight at 4°C. Immunoprecipitated RNA was utilized for qRT-PCR to determine miR-361-3p, circ_0006089, and TGFB1 expression levels.

2.6 | Colony formation assay

Transfected GC cells were reseeded into 6-well plates (200 cells/well). After culturing for 14 days at 37°C, the colonies were fixed using crystal violet. The number of colonies was counted under a microscope.

2.7 | EdU assay

In accordance with the instructions in the Cell-Light™ EdU Apollo567 *In Vitro* Imaging Kit (RiboBio), transfected GC cells in 96-well plates (1×10^4 cells/well) were stained with the EdU solution, Apollo567 solution and 4′,6-diamidino-2-phenylindole (DAPI) solution one by one. Signals were observed under a fluorescence microscope, and ImageJ software was used to analyze the EdU-positive (EdU^+) cell rate.

2.8 | Transwell assay

In a migration assay, transfected GC cells (1×10^5 cells/chamber) suspended in serum-free medium were inoculated into the upper chambers of transwell plates (24-well; BD Biosciences, San Jose, CA, USA), and complete medium was added to the lower chamber. After 24 h incubation, cells were fixed in paraformaldehyde and stained with crystal violet, and then five fields were randomly selected under a microscope (×100 magnification) for observation and counting. In the invasion assay, GC cells (4×10^5 cells/chamber) were seeded into the upper chamber which had been pre-coated with a Matrigel. The other steps were the same as those for detecting migration.

2.9 | Cell glycolysis assay

Following the instructions from the Glucose Assay Kit (Elabscience), Lactate Assay Kit (Elabscience) and ATP Assay Kit (Beyotime), GC cell glucose consumption, lactate production, and ATP levels were determined, respectively.

2.10 | Western blot analysis

Protein extraction was performed using RIPA Lysis Buffer (Beyotime) containing protease inhibitors. After quantification using the BCA Kit (Beyotime), protein (30 μg) was separated using 10% sodium dodecyl sulfate–polyacrylamide gel electrophoresis (SDS-PAGE) gel and transferred to polyvinylidene fluoride (PVDF) membrane followed by treatment with 5% non-fat dried milk for 2 h. Then, the membrane was incubated with primary antibodies (Abcam), including anti-HK2 (1:1,000, ab209847), anti-TGFB1 (1:1,000, ab92486), or anti-β-actin (1:1,000, ab8227) overnight at 4°C. After treatment with secondary antibody (1:50,000, ab97051) for 1 h at room temperature, the membrane was subjected to the enhanced chemiluminescence kit (Beyotime) to observe the protein signal. Relative protein expression was analyzed using ImageJ software.

2.11 | Flow cytometry

Transfected GC cells were stained with annexin V-FITC and propidium iodide (PI) (Dojindo). The treated cells were analyzed using a flow cytometer and the cell apoptosis rate (%; annexin V^+/PI^- and annexin V^+/PI^+) was determined using FlowJo software.

2.12 | Tube formation assay

After transfection, the supernatants of GC cells were mixed with fresh medium to prepare conditioned medium. Human umbilical vein endothelial cells (HUVECs) (Procell) were suspended in conditioned

medium and then seeded into 24-well plates that had been coated with Matrigel. After 48 h, tube formation was observed under a microscope, and tube formation rate was calculated using ImageJ software.

2.13 | Xenograft tumor models

BALB/c nude mice (Vital River, Beijing, China) were randomly divided into six groups ($n = 6$/group). GC cells were infected with lentiviruses (sh-circ_0006089: sense, 5′-CCGGACATCTGAGCTGCTGGCTAACCTCGAGGTTAGCCAGCAGCTCAGATGTTTTTTG-3′; antisense, 5′-AATTCAAAAAACATCTGAGCTGCTGGCTAACCTCGAGGTTAGCCAGCAGCTCAGATGT-3′; sh-NC: 5′-CCGGTTCTCCGAACGTGTCACGTAACTCGAGTTACGTGACACGTTCGGAGAATTTTTG-3′) with 8 mg/ml polybrene using the ViraPower Packaging Mix (Invitrogen). Then, the stable cells were obtained by treatment with 2 μg/ml puromycin for 3 days. GC cells stably transfected with sh-circ_0006089/sh-NC were collected and suspended with phosphate-buffered saline (PBS). The suspensions (2×10^6 cells/0.2 ml PBS) of cells with different transfection were injected into the right flank of BALB/c nude mice. Tumor volume was calculated every week, and the tumors were removed for weighing after 4 weeks. Tumor tissue was used for qRT-PCR, WB analysis, and immunohistochemistry (IHC) staining (for measuring Ki67-positive cells). Animal experiments were obtained by permission from the Seventh People's Hospital of Shanghai University of Traditional Chinese Medicine.

2.14 | Statistical analysis

Data were expressed as mean ± standard deviation (SD), and the differences among groups were assessed using Student t test or ANOVA. Statistical analyses were conducted using GraphPad Prism 7.0 software. A p-value < 0.05 was considered statistically significant.

3 | RESULTS

3.1 | The high expression of circ_0006089 was discovered in GC tissues and cells

Figure 1A shows the top 10 high-expression and 10 low-expression circRNAs with the largest differential expression in GC tumor tissues and normal tissues that were screened by the GSE83521 database,

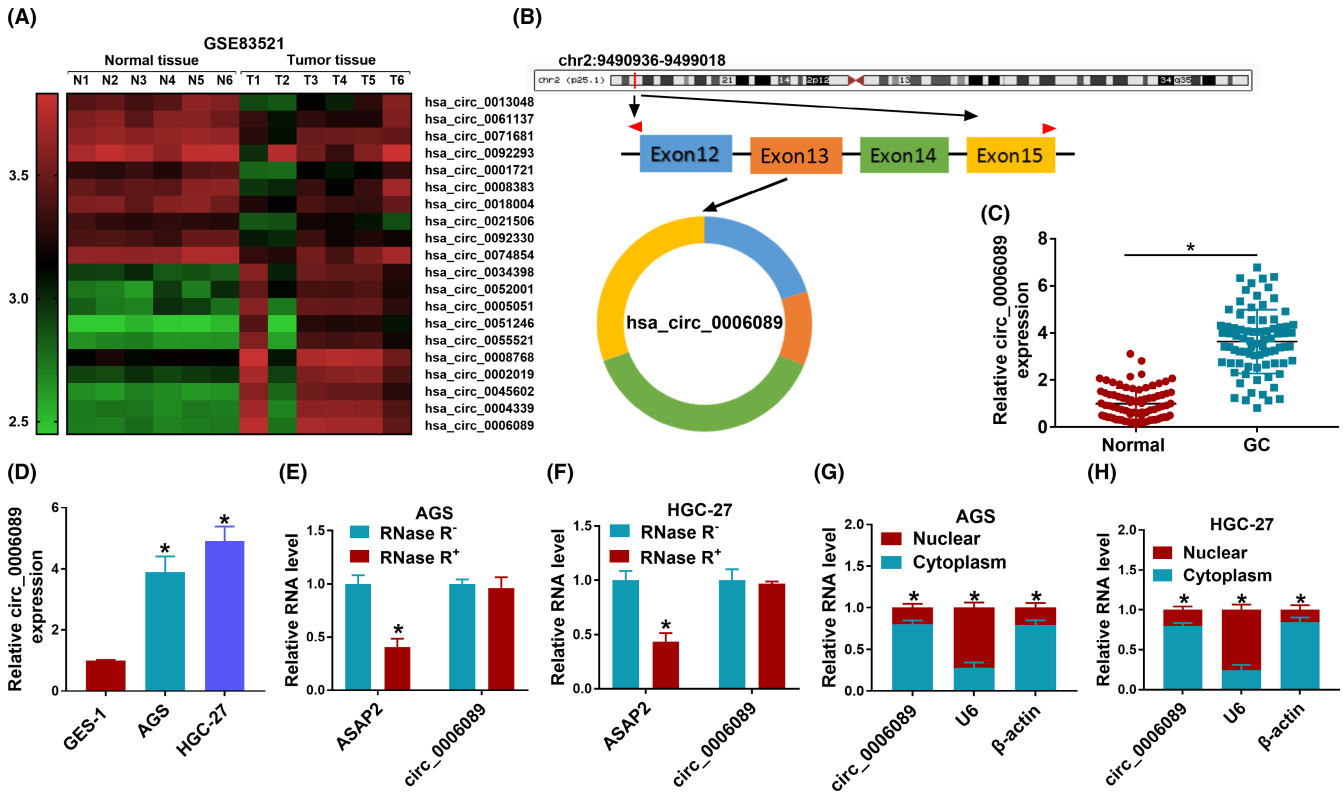

FIGURE 1 The expression of circ_0006089 in gastric cancer (GC) tissues and cells. (A) The largest differentially expressed circRNA in GC tumor tissues ($n = 6$) and normal tissues ($n = 6$) were screened against the GSE83521 database. (B) The basic information for circ_0006089 is shown. (C) circ_0006089 expression in GC tissues ($n = 80$) and adjacent normal tissues ($n = 80$) was detected using qRT-PCR. (D) circ_0006089 expression in GC cells and GES-1 cells was measured using qRT-PCR ($n = 3$). (E, F) RNase R assay was performed to confirm the resistance of circ_0006089 to RNase R digestion ($n = 3$). (G, H) Subcellular localization analysis was utilized for detecting the distribution of circ_0006089 in the cell nucleus and the cytoplasm ($n = 3$). *$p < 0.05$

among which circ_0006089 was highly expressed in GC tumor tissues. circ_0006089 is located in chr2:9490936–9499018 with a 438-bp length and is formed by the back splicing of exons 12–15 of the *ASAP2* gene (Figure 1B). Through qRT-PCR, we confirmed that circ_0006089 was upregulated in GC tissues compared with adjacent normal tissues (Figure 1C). In addition, circ_0006089 also had an elevated expression in GC cells compared with that in GES-1 cells (Figure 1D). Furthermore, we found that circ_0006089 could resist the digestion by RNase R and was mainly distributed in the cell cytoplasm (Figure 1E–H), confirming that circ_0006089 had a circular structure and might be mainly involved in post-transcriptional regulation.

3.2 | circ_0006089 serves as an miR-361-3p sponge

Bioinformatics software (starBase 3.0 and CircInteractome) was used to predict downstream miRNAs of circ_0006089 and, in total, four candidate miRNAs were found (Figure 2A). After confirming that si-circ_0006089#1/#2 indeed reduced the expression of circ_0006089 (Figure 2B), we detected the effect of circ_0006089 knockdown on the expression of candidate miRNAs. It was found that circ_0006089 knockdown had the most significant promotion effect on miR-361-3p expression in AGS and HGC-27 cells (Figure 2C,D). Therefore, miR-361-3p was selected for our research. qRT-PCR was used to detect the expression of miR-361-3p in GC tumor tissues, and it was found that miR-361-3p expression was downregulated in GC tumor tissues and was negatively correlated with circ_0006089 expression (Figure 2E,F). Also, low expression of miR-361-3p was observed in GC cells compared with GES-1 cells (Figure 2G). According to the binding sequences, we constructed the circ_0006089-WT/MUT vectors (Figure 2H). Further analysis revealed that the miR-361-3p mimic inhibited the luciferase activity of circ_0006089-WT vector rather than the circ_0006089-MUT vector (Figure 2I,J). In addition, we also detected that the enrichments of circ_0006089 and miR-361-3p were significantly increased in Ago2 (Figure 2K,L). These results confirmed the interaction between circ_0006089 and miR-361-3p.

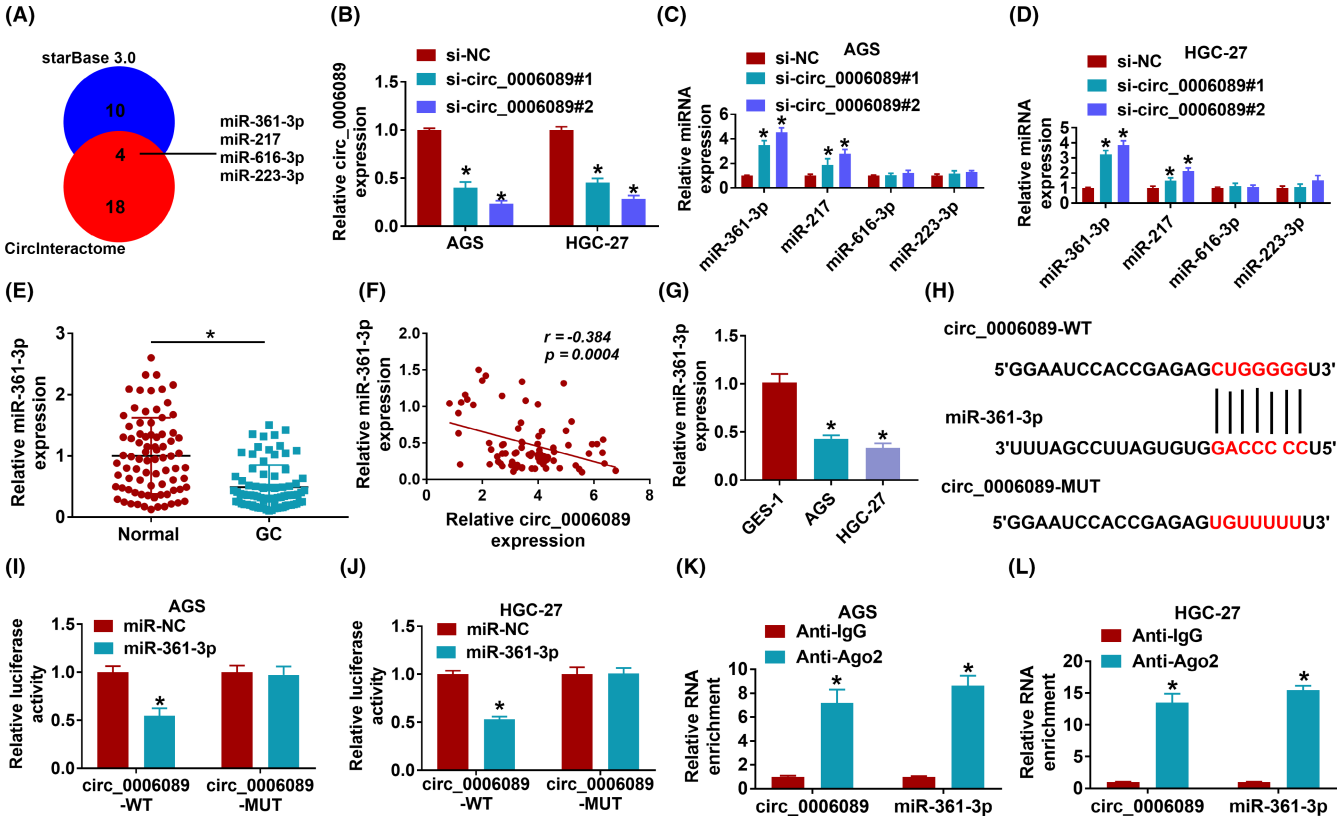

FIGURE 2 circ_0006089 serves as an miR-361-3p sponge. (A) starBase 3.0 and CircInteractome software were used to predict the targeted miRNA for circ_0006089. (B) Transfection efficiency of si-circ_0006089#1/#2 was confirmed using qRT-PCR ($n = 3$). (C, D) Candidate miRNA expression in GC cells transfected with si-circ_0006089#1/#2 or si-NC was measured using qRT-PCR ($n = 3$). (E) The miR-361-3p expression in GC tissues ($n = 80$) and adjacent normal tissues ($n = 80$) was detected using qRT-PCR. (F) Pearson correlation analysis was used to analyze linear correlation ($n = 80$). (G) The miR-361-3p expression in GC cells and GES-1 cells was measured using qRT-PCR ($n = 3$). (H) The sequences of circ_0006089-WT/MUT are presented. Dual-luciferase reporter assay (I, J) and RIP assay (K, L) were used to confirm the interaction between them ($n = 3$). $^*p < 0.05$

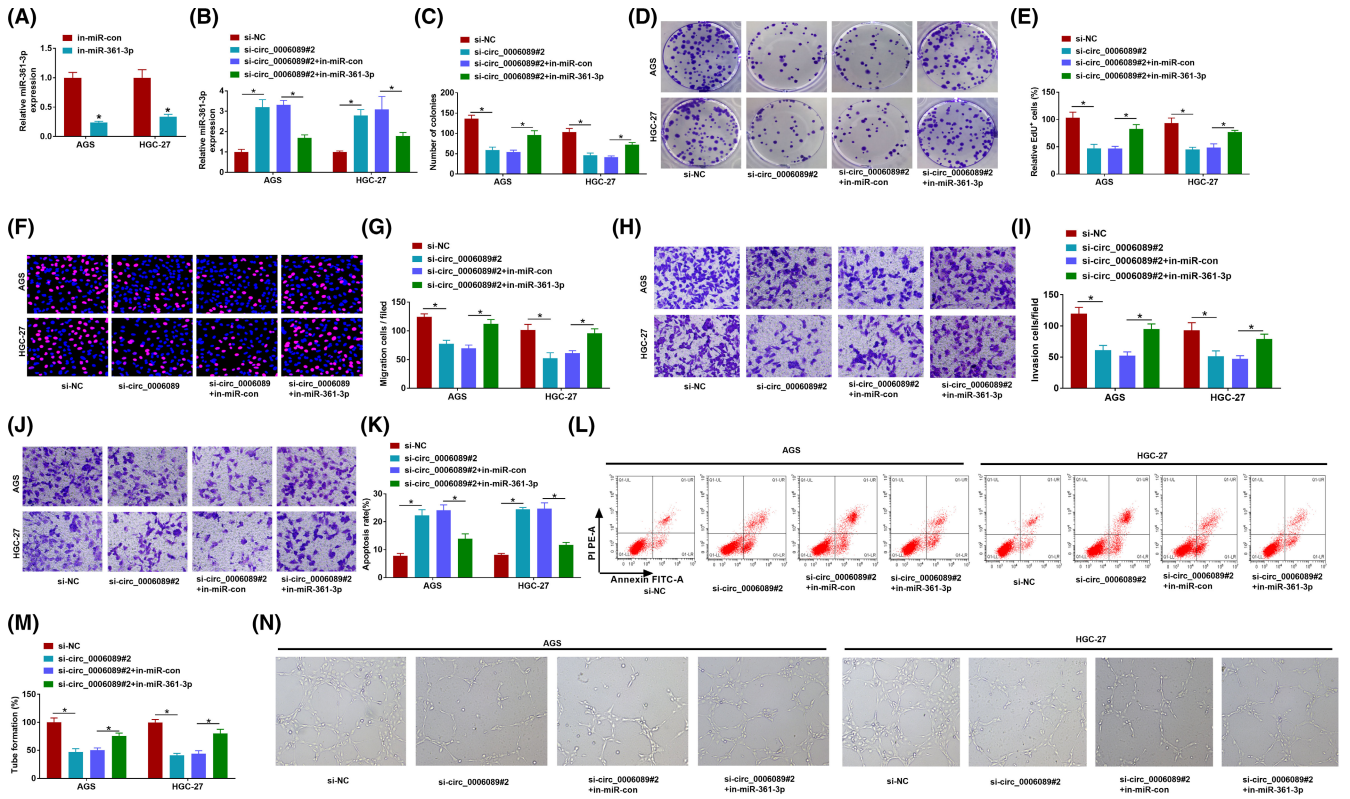

FIGURE 3 circ_0006089 knockdown suppressed GC cell progression by sponging miR-361-3p. (A) The transfection efficiency of in-miR-361-3p was assessed using qRT-PCR ($n = 3$). (B–N) AGS and HGC-27 cells were transfected with si-circ_0006089#2 and in-miR-361-3p ($n = 3$). (B) miR-361-3p expression was determined using qRT-PCR. Colony formation assay (C, D), EdU assay (E, F), and transwell assay (G–J) were used to measure cell proliferation, migration, and invasion, respectively. Flow cytometry (K, L) and tube formation assay (M, N) were performed to evaluate cell apoptosis and angiogenesis, respectively. $^*p < 0.05$

3.3 | circ_0006089 knockdown suppressed GC cell growth, metastasis, glycolysis, and angiogenesis by sponging miR-361-3p

As the inhibitory effect of si-circ_0006089#2 on circ_0006089 expression and the promotion effect on miR-361-3p expression was better than si-circ_0006089#1 (Figure 2B–D), si-circ_0006089#2 was selected for subsequent functional tests. After confirmation that in-miR-361-3p indeed decreased miR-361-3p expression in AGS and HGC-27 cells (Figure 3A), we co-transfected with si-circ_0006089#2 and in-miR-361-3p into GC cells to verify whether circ_0006089 sponged miR-361-3p to participate in the regulation of GC progression. We found that the increasing effect of circ_0006089 knockdown on miR-361-3p expression could be inhibited by in-miR-361-3p (Figure 3B). Function analysis suggested that circ_0006089 silencing could repress the number of colonies, EdU^+ cell rates, migration cells, and invasion cells, while these effects were reversed by the addition of in-miR-361-3p (Figure 3C–J). Furthermore, interference of circ_0006089 enhanced the apoptosis rate and reduced the tube formation rate of AGS and HGC-27 cells, whereas miR-361-3p inhibitor eliminated these effects (Figure 3K–N). Also, miR-361-3p inhibitor revoked the suppressive effects of circ_0006089 knockdown on glucose consumption, lactate production, ATP level, and HK2 protein expression in AGS and HGC-27 cells (Figure S1A–D). The above data revealed that circ_0006089 might promote GC cell growth, metastasis, glycolysis, and angiogenesis through sponging miR-361-3p.

3.4 | TGFB1 was targeted by miR-361-3p

Using multiple bioinformatics analysis software (starBase3.0, TargetScan7.1, miRDB and GSE54129), we predicted the target of miR-361-3p and found that only TGFB1 could be predicted jointly (Figure 4A). In the GSE54129 database, TGFB1 mRNA expression was found to be upregulated in GC tumor tissues compared with normal tissues (Figure 4B). Here, we measured TGFB1 expression in GC tissues and adjacent normal tissues and confirmed that TGFB1 had increased expression levels in GC tissues and was negatively correlated with miR-361-3p expression (Figure 4C,D). At the protein level, TGFB1 expression was higher in GC tissues and cells than that in adjacent normal tissues and GES-1 cells, respectively (Figure 4E,F). Then, we determined that the miR-361-3p mimic could promote miR-361-3p expression in AGS and HGC-27 cells (Figure 4G), and found that the miR-361-3p mimic markedly reduced TGFB1 protein expression (Figure 4H). Then, the TGFB1 3′UTR-WT/MUT vectors were generated to perform dual-luciferase reporter assays (Figure 4I). The results indicated that only the luciferase activity driven by the TGFB1 3′UTR-WT vector could be decreased by

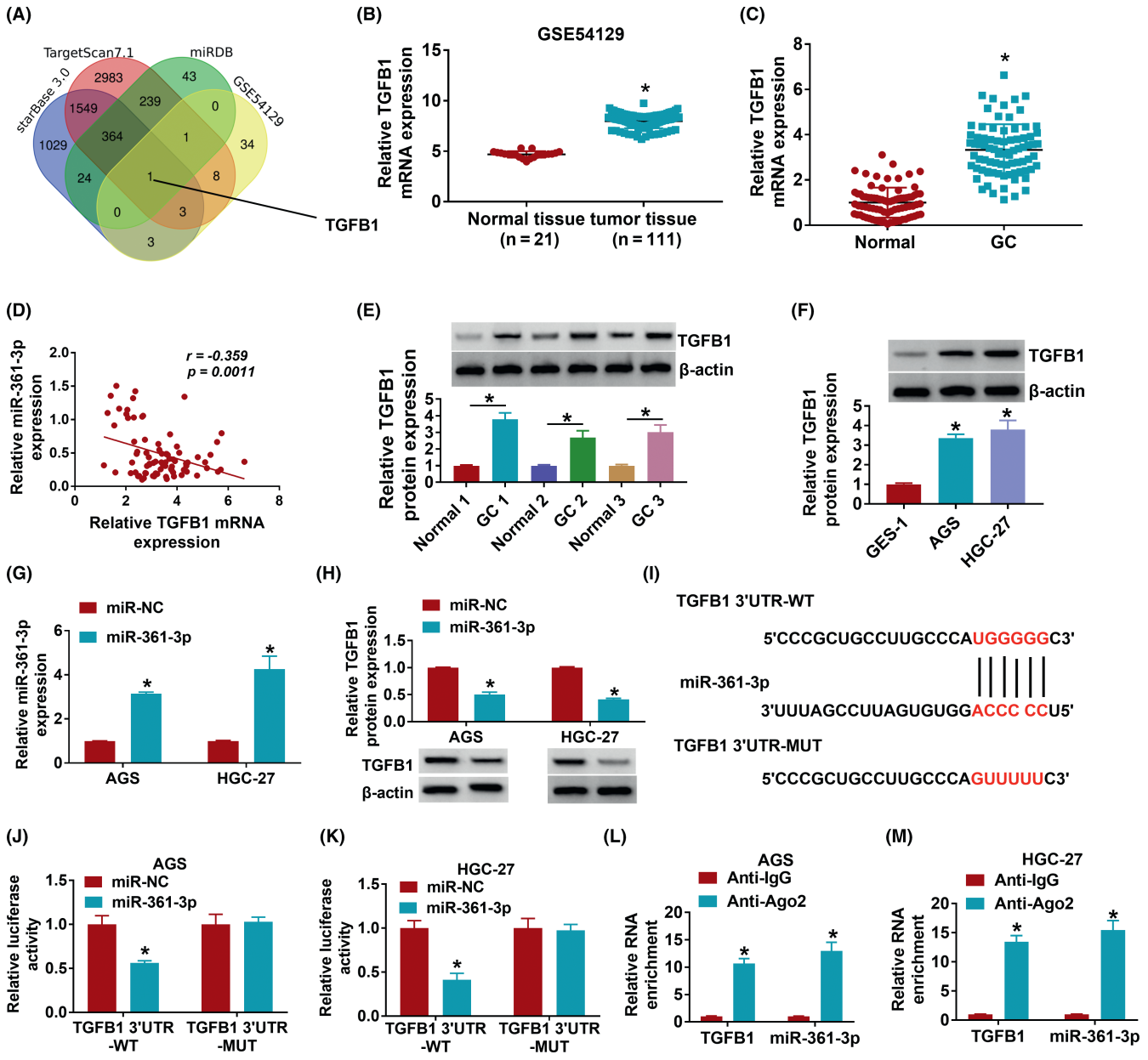

FIGURE 4 TGFB1 was targeted by miR-361-3p. (A) Venn diagram shows the predicted targets of miR-361-3p. (B) The TGFB1 expression in GC tumor tissues ($n = 21$) and normal tissues ($n = 111$) was analyzed in the GSE54129 database. (C) The TGFB1 expression was detected using qRT-PCR in GC tissues ($n = 80$) and adjacent normal tissues ($n = 80$). (D) Linear correlation was analyzed using Pearson correlation analysis ($n = 80$). (E, F) The TGFB1 protein expression in GC tissues and cells was measured using western blot (WB) analysis ($n = 3$). (G) The transfection efficiency of miR-361-3p mimic was tested using qRT-PCR ($n = 3$). (H) TGFB1 protein expression was determined using WB analysis in GC cells transfected with miR-361-3p mimic or miR-NC ($n = 3$). (I) The sequences of TGFB1 3′UTR-WT/MUT vectors are shown. The interaction between them was confirmed using a dual-luciferase reporter assay (J, K) and RIP assay (L, M) ($n = 3$). $^*p < 0.05$

the miR-361-3p mimic (Figure 4J,K). Also, the levels of TGFB1 and miR-361-3p were found to be enriched in Ago2 (Figure 4L,M). The above results suggested that miR-361-3p could target TGFB1.

3.5 | miR-361-3p inhibited GC progression by targeting TGFB1

In subsequently experiments, we performed rescue experiments to confirm that miR-361-3p targeted TGFB1 to regulate GC progression. Transfection of the TGFB1 overexpression vector indeed enhanced TGFB1 protein expression in AGS and HGC-27 cells (Figure 5A). After that, we assessed the function of GC cells transfected with the miR-361-3p mimic and the TGFB1 overexpression vector. The inhibiting effects of miR-361-3p mimic on TGFB1 protein expression were promoted by the addition of the TGFB1 overexpression vector (Figure 5B). As a results, miR-361-3p suppressed the number of colonies, EdU^+ cell rates, migration cells, invasion cells, glucose consumption, lactate production, ATP level, and HK2 protein expression in AGS and HGC-27 cells, whereas these effects

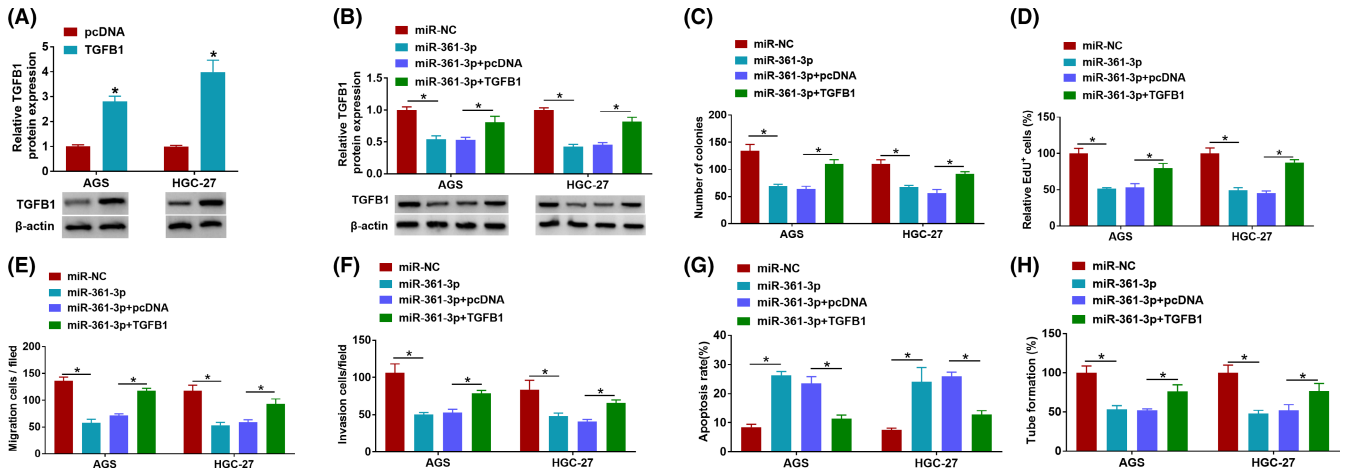

FIGURE 5 miR-361-3p inhibited GC progression using targeting TGFB1. (A) The transfection efficiency of TGFB1 overexpression vector was confirmed using western blot (WB) analysis ($n = 3$). (B–H) AGS and HGC-27 cells were transfected with miR-361-3p mimic and TGFB1 overexpression vector ($n = 3$). (B) TGFB1 protein expression was detected using WB analysis. Cell proliferation, migration, and invasion were determined using colony formation assay (C), EdU assay (D) and transwell assay (E, F), respectively. Cell apoptosis and angiogenesis were evaluated using flow cytometry (G) and tube formation assay (H), respectively. $^*p < 0.05$

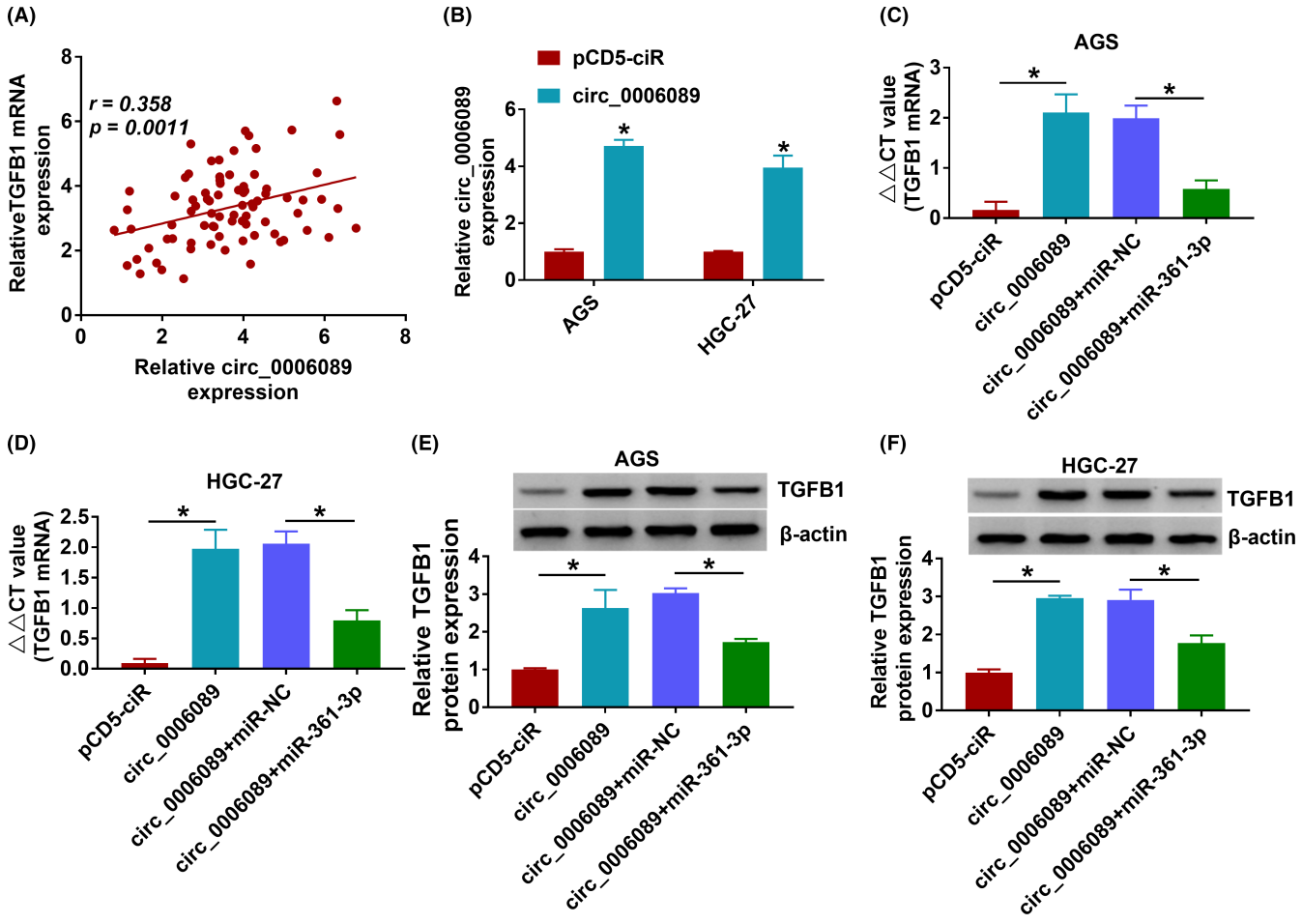

FIGURE 6 circ_0006089 sponged miR-361-3p to promote TGFB1 expression. (A) Pearson correlation analysis was used to assess linear correlation between TGFB1 and circ_0006089 expression in GC tissues ($n = 80$). (B) The transfection efficiency of pCD5 circ_0006089 overexpression vector was assessed by qRT-PCR ($n = 3$). (C–F) TGFB1 mRNA and protein expression was detected using qRT-PCR and western blot (WB) analysis in GC cells transfected with pCD5 circ_0006089 overexpression vector and miR-361-3p mimic ($n = 3$). $^*p < 0.05$

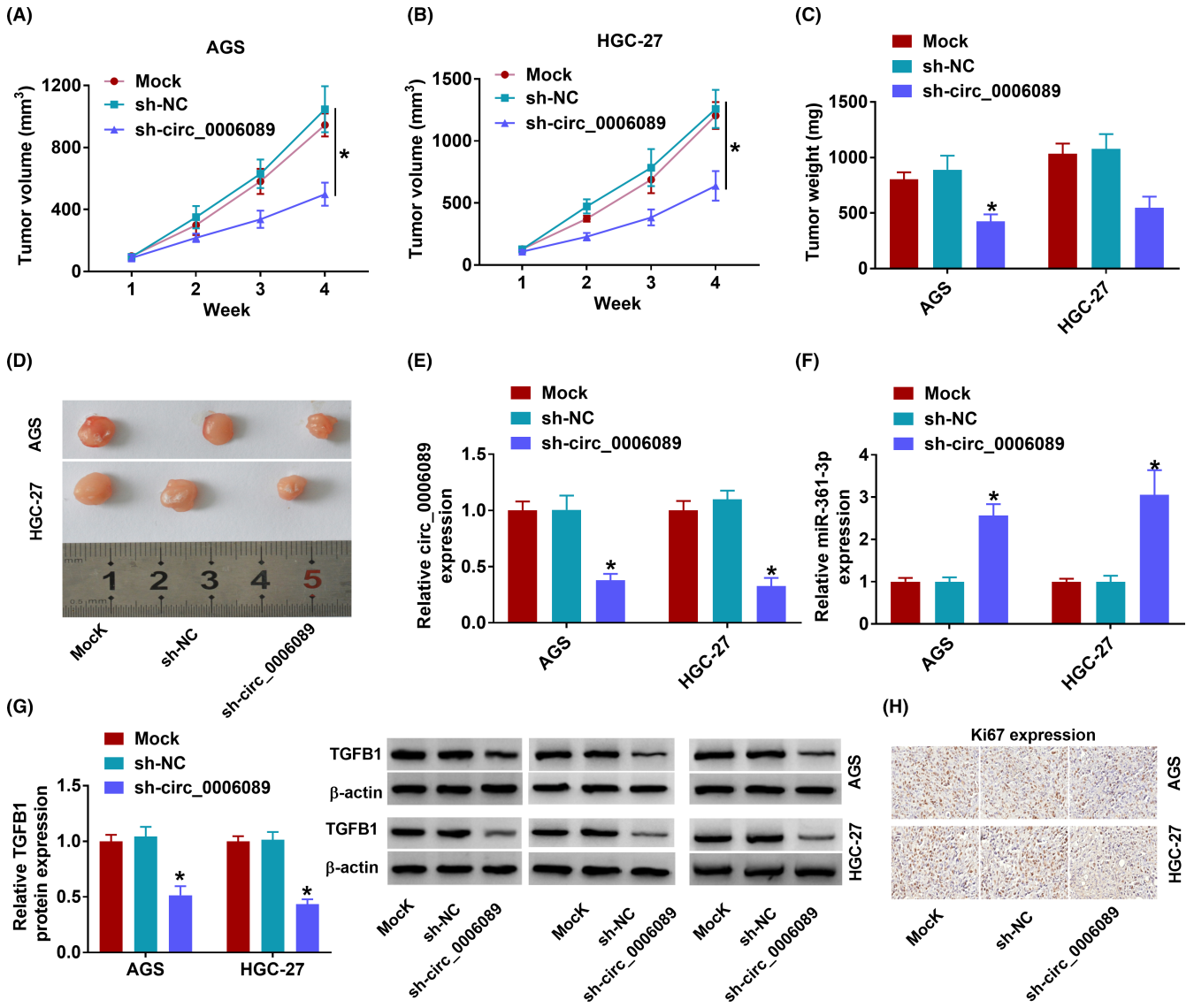

FIGURE 7 Interference of circ_0006089 restrained GC tumorigenesis. AGS and HGC-27 cells transfected with or without sh-NC or sh-circ_0006089 were injected into nude mice ($n = 6$). Tumor volume (A, B) and tumor weight (C) were determined. (D) Tumor pictures for each group are shown. (E–G) The circ_0006089, miR-361-3p, and TGFB1 expression in the tumor tissues was detected using qRT-PCR and western blot (WB) analysis. (H) IHC staining was used to measure Ki67-positive cells in tumor tissues. *$p < 0.05$

could be reversed by overexpressing TGFB1 (Figures 5C–F and S1E-H). Moreover, upregulated miR-361-3p also promoted the apoptosis rate and inhibited the tube formation rate of AGS and HGC-27 cells. However, these effects also were overturned by TGFB1 overexpression (Figure 5G,H). All results illuminated that miR-361-3p repressed GC cell growth, metastasis, glycolysis, and angiogenesis by targeting TGFB1.

3.6 | Circ_0006089 sponged miR-361-3p to promote TGFB1 expression

In GC tissues, we found that TGFB1 mRNA expression was positively correlated with circ_0006089 expression (Figure 6A). Then, the pCD5 circ_0006089 overexpression vector was used to increase circ_0006089 expression in AGS and HGC-27 cells (Figure 6B). Further analysis indicated that circ_0006089 overexpression significantly enhanced TGFB1 expression in AGS and HGC-27 cells at the mRNA and protein levels, whereas these effects could be abolished by the miR-361-3p mimic (Figure 6C–F). Therefore, we confirmed that circ_0006089 positively regulated TGFB1 by sponging miR-361-3p.

3.7 | Interference of circ_0006089 restrained GC tumorigenesis

To further determine the role of circ_0006089 in GC progression, we explored the function of sh-circ_0006089 in GC tumorigenesis *in vivo*. After AGS and HGC-27 cells transfected with sh-circ_0006089

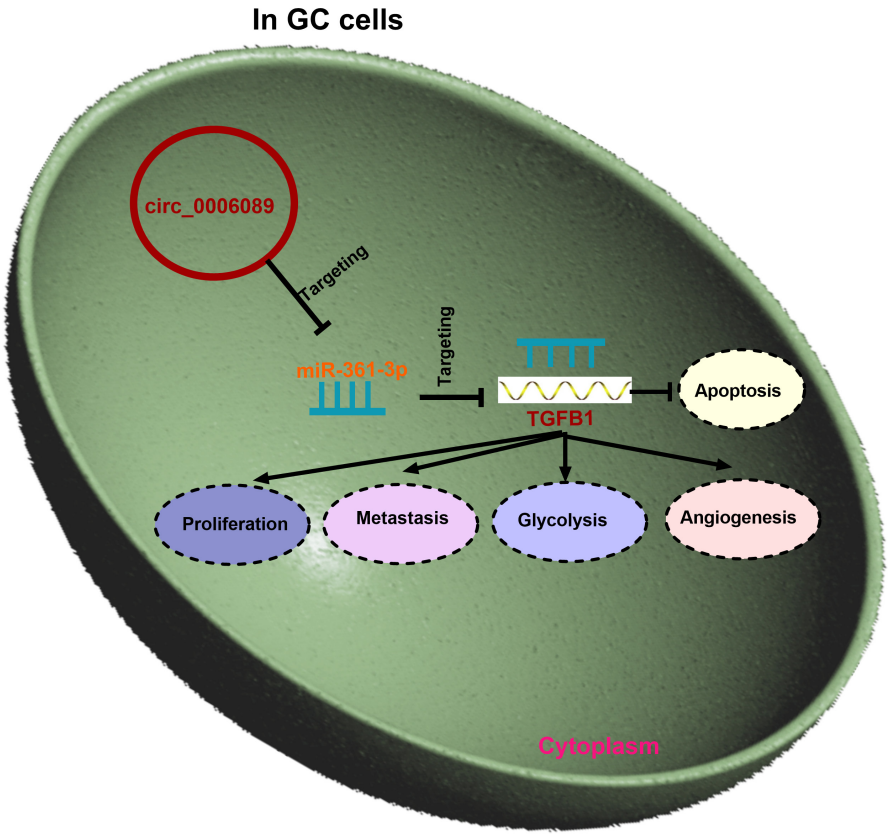

FIGURE 8 The mechanism diagram of this study. circ_0006089 sponged miR-361-3p to regulate TGFB1, thereby promoting GC cell proliferation, metastasis, glycolysis, angiogenesis, and decreasing apoptosis

were injected into nude mice, we discovered that the tumor volume and weight were markedly reduced compared with the control groups (Figure 7A–C). As shown in Figure 7D, the tumor size in the sh-circ_0006089 group was significantly smaller than that in the control groups. The tumor tissues were collected for qRT-PCR and WB analysis, and the results showed that circ_0006089 expression was decreased, miR-361-3p expression was enhanced, and TGFB1 protein expression was inhibited in the sh-circ_0006089 group (Figure 7E–G). Also, we observed that the positive cells of proliferation marker Ki67 were reduced in the tumor tissues of the sh-circ_0006089 group (Figure 7H), confirming that circ_0006089 knockdown repressed tumor cell proliferation. In addition, we also used sh-circ_0006089 and in-miR-361-3p to perform *in vitro* experiments. After confirming that sh-circ_0006089 reduced circ_0006089 expression and in-miR-361-3p decreased miR-361-3p expression in GC cells (Figure S2A,B), we co-transfected with sh-circ_0006089 and in-miR-361-3p into GC cells. The addition of in-miR-361-3p suppressed miR-361-3p expression promoted by sh-circ_0006089 (Figure S2C). Our data showed that sh-circ_0006089 hindered the number of colonies, EdU^+ cell rates, migration, invasion, glucose consumption, lactate production, ATP level, and HK2 protein expression, whereas these effects were reversed by miR-361-3p inhibitor (Figure S2D–O). Moreover, sh-circ_0006089 also enhanced the apoptosis rate and suppressed tube formation, and the miR-361-3p inhibitor also overturned these effects (Figure S2P–S). Above all, we pointed out that circ_0006089 regulated the miR-361-3p/TGFB1 axis to promote GC progression by increasing cell proliferation, metastasis, glycolysis, angiogenesis, and decreasing apoptosis (Figure 8).

4 | DISCUSSION

More and more studies have confirmed that glycolysis is an important source of energy acquisition for tumor cells.[17,18] Glycolysis is a common process of energy metabolism in living organisms, which refers to the process of converting glucose into lactic acid and producing a small amount of ATP under the conditions of insufficient oxygen.[19,20] Therefore, measuring glucose consumption, lactate production, and ATP levels to assess the glycolysis capacity of cells is an effective indicator of cell function. Here, we assessed the effect of circ_0006089 on glucose consumption, lactate production, and ATP levels, which could accurately reflect the effects of circ_0006089 on GC cell function.

circRNA is considered to be a potentially attractive biomarker in human cancers due to its special structure. The regulatory role of circRNA in cancer development has been widely confirmed. Of course, different circRNAs have also been shown to have different effects. Some circRNAs mediate the progression of GC as tumor-promoting factors, such as circ-0002570[21] and circC6orf132,[22] and some mediate GC development as tumor-inhibiting factors, such as circ-TNPO3[23] and circGSK3B.[24] In this, the role of highly expressed circ_0006089 in GC progression was verified. We discovered that circ_0006089 interference restrained GC cell growth, metastasis, glycolysis, and angiogenesis, as well as reduced tumor growth. These data showed that circ_0006089 exerted an oncogenic role in GC, which was consistent with the former studies.[16]

The hypothesis of ceRNA provides the direction for revealing the mechanism of circRNAs.[9,10] Here, miR-361-3p was confirmed to be sponged by circ_0006089. Studies had indicated that circ_0011385

inhibited miR-361-3p to promote hepatocellular carcinoma proliferation.[25] miR-361-3p had been determined to be a tumor suppressor in cervical cancer, which could suppress cancer cell viability and metastasis.[26] Many research confirmed that miR-361-3p exerted suppressive effects on GC cell growth and metastasis, as well as angiogenesis.[27,28] A recent study revealed that circTMC5 targeted miR-361-3p to reduce its expression, thereby accelerating GC cell proliferation and metastasis.[29] Here, the miR-361-3p mimic markedly repressed GC cell growth, metastasis, glycolysis, and angiogenesis, and its inhibitor also revoked the function of si-circ_0006089#2 in GC cells. This data not only confirmed the anti-tumor role of miR-361-3p in GC, but also confirmed that circ_0006089 indeed promoted the malignant phenotype of GC via targeting miR-361-3p.

TGFB1 belongs to the TGFB subfamily, which is widely involved in various physiological processes, such as angiogenesis, immune diseases, and cancer development.[30-32] Elevated TGFB1 expression has been found to lead to breast cancer cell growth and metastasis.[33] Studies have shown that estrogenic signals accelerated endometrial cancer cell metastasis by increasing TGFB1 expression.[34] In GC-related studies, TGFB1 expression was higher in cancer tissues, and TGFB1 activation was considered to be related to GC migration and invasion.[35,36] The polymorphism of TGFB1 has been confirmed to act as a prognostic biomarker of gastric adenocarcinoma.[37] In this, TGFB1 was confirmed to be upregulated in GC tissues and was verified to be targeted by miR-361-3p. Overexpressed TGFB1 abolished the inhibitory function of miR-361-3p on GC cell progression, showing that miR-361-3p indeed targeted TGFB1, a tumor promoter, to hinder GC development. In addition, our data showed that circ_0006089 had a positively regulation on TGFB1 expression, confirming the existence of the circ_0006089/miR-361-3p/TGFB1 pathway.

In summary, our study suggested that circ_0006089 facilitated GC cell growth, metastasis, glycolysis, and angiogenesis through regulating the miR-361-3p/TGFB1 pathway. Therefore, our study revealed that circ_0006089 served as an oncogene to mediate the GC malignant phenotype. These results deepen our understanding of the pathogenesis of GC and provide a theoretical basis for circ_0006089 as a potential therapeutic target for GC.

DISCLOSURE

The authors declare that they have no conflict of interest.

ORCID

Qihua Xu https://orcid.org/0000-0001-9976-9159

REFERENCES

1. Smyth EC, Nilsson M, Grabsch HI, et al. Gastric cancer. *Lancet*. 2020;396(10251):635-648.
2. Petryszyn P, Chapelle N, Matysiak-Budnik T. Gastric cancer: Where are we heading? *Dig Dis*. 2020;38(4):280-285.
3. Song Z, Wu Y, Yang J, et al. Progress in the treatment of advanced gastric cancer. *Tumour Biol*. 2017;39(7):1010428317714626.
4. Digklia A, Wagner AD. Advanced gastric cancer: Current treatment landscape and future perspectives. *World J Gastroenterol*. 2016;22(8):2403-2414.
5. Patel TH, Cecchini M. Targeted therapies in advanced gastric cancer. *Curr Treat Options Oncol*. 2020;21(9):70.
6. Chen Z, Li Y, Tan B, et al. Progress and current status of molecule-targeted therapy and drug resistance in gastric cancer. *Drugs Today (Barc)*. 2020;56(7):469-482.
7. Chen LL. The expanding regulatory mechanisms and cellular functions of circular RNAs. *Nat Rev Mol Cell Biol*. 2020;21(8):475-490.
8. Lei M, Zheng G, Ning Q, et al. Translation and functional roles of circular RNAs in human cancer. *Mol Cancer*. 2020;19(1):30.
9. Yang G, Zhang Y, Yang J. Identification of potentially functional CircRNA-miRNA-mRNA regulatory network in gastric carcinoma using bioinformatics analysis. *Med Sci Monit*. 2019;25:8777-8796.
10. Panda AC. Circular RNAs act as miRNA sponges. *Adv Exp Med Biol*. 2018;1087:67-79.
11. Li J, Sun D, Pu W, et al. Circular RNAs in cancer: Biogenesis, function, and clinical significance. *Trends Cancer*. 2020;6(4):319-336.
12. Lei B, Tian Z, Fan W, et al. Circular RNA: a novel biomarker and therapeutic target for human cancers. *Int J Med Sci*. 2019;16(2):292-301.
13. Zhang W, Zheng M, Kong S, et al. Circular RNA hsa_circ_0007507 may serve as a biomarker for the diagnosis and prognosis of gastric cancer. *Front Oncol*. 2021;11:699625.
14. Cui Y, Cao J, Huang S, et al. circRNA_0006470 promotes the proliferation and migration of gastric cancer cells by functioning as a sponge of miR-27b-3p. *Neoplasma*. 2021;68(6):1245-1256.
15. Gao L, Xia T, Qin M, et al. CircPTK2 suppresses the progression of gastric cancer by targeting the MiR-196a-3p/AATK Axis. *Front Oncol*. 2021;11:706415.
16. Sun Y, Ma J, Lin J, et al. Circular RNA circ_ASAP2 regulates drug sensitivity and functional behaviors of cisplatin-resistant gastric cancer cells by the miR-330-3p/NT5E axis. *Anticancer Drugs*. 2021;32(9):950-961.
17. Ganapathy-Kanniappan S, Geschwind JF. Tumor glycolysis as a target for cancer therapy: progress and prospects. *Mol Cancer*. 2013;12:152.
18. Moreno-Sanchez R, Rodriguez-Enriquez S, Marin-Hernandez A, et al. Energy metabolism in tumor cells. *FEBS J*. 2007;274(6):1393-1418.
19. Chaudhuri AD, Kabaria S, Choi DC, et al. MicroRNA-7 promotes glycolysis to protect against 1-Methyl-4-phenylpyridinium-induced cell death. *J Biol Chem*. 2015;290(19):12425-12434.
20. Guo W, Qiu Z, Wang Z, et al. MiR-199a-5p is negatively associated with malignancies and regulates glycolysis and lactate production by targeting hexokinase 2 in liver cancer. *Hepatology*. 2015;62(4):1132-1144.
21. Yang L, Zhou YN, Zeng MM, et al. Circular RNA Circ-0002570 accelerates cancer progression by regulating VCAN via MiR-587 in gastric cancer. *Front Oncol*. 2021;11:733745.
22. Chen W, Ji Y. CircC6orf132 facilitates proliferation, migration, invasion, and glycolysis of gastric cancer cells under hypoxia by acting on the miR-873-5p/PRKAA1 Axis. *Front Genet*. 2021;12:636392.
23. Yu T, Ran L, Zhao H, et al. Circular RNA circ-TNPO3 suppresses metastasis of GC by acting as a protein decoy for IGF2BP3 to regulate the expression of MYC and SNAIL. *Mol Ther Nucleic Acids*. 2021;26:649-664.
24. Ma X, Chen H, Li L, et al. CircGSK3B promotes RORA expression and suppresses gastric cancer progression through the prevention of EZH2 trans-inhibition. *J Exp Clin Cancer Res*. 2021;40(1):330.
25. Ni C, Yang S, Ji Y, et al. Hsa_circ_0011385 knockdown represses cell proliferation in hepatocellular carcinoma. *Cell Death Discov*. 2021;7(1):270.
26. Li C, Li Y, Zhang Y, et al. Knockdown of LINC01123 inhibits cell viability, migration and invasion via miR-361-3p/TSPAN1 targeting in cervical cancer. *Exp Ther Med*. 2021;22(4):1184.
27. Cui X, Zhang H, Chen T, et al. Long noncoding RNA SNHG22 induces cell migration, invasion, and angiogenesis of gastric cancer cells

via microRNA-361-3p/HMGA1/Wnt/beta-Catenin Axis. *Cancer Manag Res*. 2020;12:12867-12883.
28. Xin H, Yan Z, Cao J. Long non-coding RNA ABHD11-AS1 boosts gastric cancer development by regulating miR-361-3p/PDPK1 signalling. *J Biochem*. 2020;168(5):465-476.
29. Xu P, Xu X, Wu X, et al. CircTMC5 promotes gastric cancer progression and metastasis by targeting miR-361-3p/RABL6. *Gastric Cancer*. 2022;25(1):64-82.
30. Yang Y, Zhang N, Lan F, et al. Transforming growth factor-beta 1 pathways in inflammatory airway diseases. *Allergy*. 2014;69(6):699-707.
31. Tang RZ, Gu SS, Chen XT, et al. Immobilized transforming growth factor-beta 1 in a stiffness-tunable artificial extracellular matrix enhances mechanotransduction in the epithelial mesenchymal transition of hepatocellular carcinoma. *ACS Appl Mater Interfaces*. 2019;11(16):14660-14671.
32. Elimelech R, Khoury N, Tamari T, et al. Use of transforming growth factor-beta loaded onto beta-tricalcium phosphate scaffold in a bone regeneration rat calvaria model. *Clin Implant Dent Relat Res*. 2019;21(4):593-601.
33. Mishra AK, Parish CR, Wong ML, et al. Leptin signals via TGFB1 to promote metastatic potential and stemness in breast cancer. *PLoS One*. 2017;12(5):e0178454.
34. Huang X, Wang X, Shang J, et al. Estrogen related receptor alpha triggers the migration and invasion of endometrial cancer cells via up regulation of TGFB1. *Cell Adh Migr*. 2018;12(6):538-547.
35. Ishimoto T, Miyake K, Nandi T, et al. Activation of transforming growth factor beta 1 signaling in gastric cancer-associated fibroblasts increases their motility, via expression of rhomboid 5 homolog 2, and ability to induce invasiveness of gastric cancer cells. *Gastroenterology*. 2017;153(1):191-204 e116.
36. Li T, Huang H, Shi G, et al. TGF-beta1-SOX9 axis-inducible COL10A1 promotes invasion and metastasis in gastric cancer via epithelial-to-mesenchymal transition. *Cell Death Dis*. 2018;9(9):849.
37. Juarez I, Gutierrez A, Vaquero-Yuste C, et al. TGFB1 polymorphisms and TGF-beta1 plasma levels identify gastric adenocarcinoma patients with lower survival rate and disseminated disease. *J Cell Mol Med*. 2021;25(2):774-783.

SUPPORTING INFORMATION

Additional supporting information may be found in the online version of the article at the publisher's website.

How to cite this article: Zhou Y, Zhang Q, Liao B, Qiu X, Hu S, Xu Q. circ_0006089 promotes gastric cancer growth, metastasis, glycolysis, and angiogenesis by regulating miR-361-3p/TGFB1. *Cancer Sci*. 2022;113:2044–2055. doi:10.1111/cas.15351